Collision-Energy-Resolved Penning Ionization Electron Spectroscopy of HCOOH, CH_3COOH, and $HCOOCH_3$ by Collision with He*(2^3S) Metastable Atoms

Andriy Borodin, Masakazu Yamazaki, Naoki Kishimoto, and Koichi Ohno*

Department of Chemistry, Graduate School of Science, Tohoku University, Aramaki, Aoba-ku, Sendai 980-8578, Japan

Received: March 10, 2005; In Final Form: April 7, 2005

Penning ionization of formic acid (HCOOH), acetic acid (CH_3COOH), and methyl formate ($HCOOCH_3$) upon collision with metastable He*(2^3S) atoms was studied by collision-energy/electron-energy-resolved two-dimensional Penning ionization electron spectroscopy (2D-PIES). Anisotropy of interaction between the target molecule and He*(2^3S) was investigated based on the collision energy dependence of partial ionization cross sections (CEDPICS) obtained from 2D-PIES as well as ab initio molecular orbital calculations for the access of a metastable atom to the target molecule. For the interaction potential calculations, a Li atom was used in place of He*(2^3S) metastable atom because of its well-known similarity in interaction with targets. The results indicate that in the studied collision energy range the attractive potential localizes around the oxygen atoms and that the potential well at the carbonyl oxygen atom is at least twice as much as that at the hydroxyl oxygen. Moreover we can notice that attractive potential is highly anisotropic. Repulsive interactions can be found around carbon atoms and the methyl group.

I. Introduction

The interaction between various atoms and molecules is important in chemistry. The knowledge about the interaction potential of molecules can be very useful for the understanding of chemical processes and reactions. As a method for obtaining some information on intermolecular interactions, chemiionization processes can be used. In the case of Penning ionization,[1−3] which is known as one of the chemiionization processes, a target molecule or atom (M) collides with a metastable atom (A*) resulting in an electron ejection:

$$A^* + M \rightarrow A + M_i^+ + e^- \quad (1)$$

The intensity of the positive ions generated in collisional ionization determines the total ionization cross section of target molecules. The ionization cross sections were studied well for many molecules in previous years.[4−11] This total ionization cross section is the sum of the partial cross sections which can be related to molecular orbitals (MOs). In the Penning ionization process, an electron in a MO having large electron densities outside the surface of M is transferred to the inner-shell orbital of A*.[12] The relative ratio of the partial ionization cross sections can be observed by an electron spectroscopic technique that is known as Penning ionization electron spectroscopy (PIES).[13]

The collision energy dependence of Penning ionization cross sections enables us to investigate the interaction potential between A* and M.[2,4] The increasing ionization cross section with the increase of collision energy indicates repulsive interaction between a metastable atom and the target, since a metastable atom with the larger kinetic energy reaches the inner region of the target against the repulsive potential with higher ionization probability. On the contrary, attractive interaction between A* and M results in decreasing ionization cross section with the increase of collision energy, which is caused by the decreasing numbers of A* trajectories deflected by the effective potential with the increase of collision energy.

Since the electron distribution of individual MOs is more or less localized on a special part of the molecule, information on the anisotropy of interaction between A* and a target molecule can be obtained by collision energy dependence of partial ionization cross sections (CEDPICS) with electron spectroscopy and a velocity selection of A*.[14−17] The time-of-flight (TOF) method was adapted in our group rather than the velocity-controlled supersonic jet beam,[18−20] since the TOF method has the advantage in measurement of collision-energy/electron-energy-resolved two-dimensional Penning ionization electron spectroscopy (2D-PIES).[21] The 2D spectrum is accumulated as a function of two parameters, kinetic energy (E_e) of ejected electrons and collision energy (E_c) between A* and M. Cuts of the 2D spectrum at selected ionization bands give CEDPICS, while cuts of the 2D spectrum at selected collision energies provide collision-energy-resolved Penning ionization electron spectra (CERPIES).

On the other hand, peak energy shift in PIES or CERPIES with respect to the ionization band in ultraviolet photoelectron spectroscopy (UPS) can provide us information on anisotropy of interactions. According to a two-potential curve model of Penning ionization processes, the electron energy E_e is equal to the energy difference, at the interdistance (R) where the excitation transfer occurs, between the incoming potential curve $V^*(R)$ for the entrance channel (A* + M) and the outgoing potential curve $V^+(R)$ for the exit channel ($A + M^+$), provided that the relative translational energy is conserved during the transfer of electronic excitation. The position of peaks measured in PIES can be analyzed therefore as follows:

$$E_e(R) = V^*(R) - V_i^+(R) = E_{A^*} - [IP_i(\infty) + \Delta IP_i(R)] \quad (2)$$

where E_{A^*} is the excitation energy of the atomic probe, A*

* Address correspondence to this author. Phone: +81-22-795-6576. Fax: +81-22-795-6580. E-mail: ohnok@qpcrkk.chem.tohoku.ac.jp.

10.1021/jp051244e CCC: $30.25
Published on Web 05/11/2005

(19.82 eV for He*(2^3S)), and $IP_i(\infty)$ is the ionization potential for the *i*th ionic state of the *isolated* molecule determined by UPS. At last, $\Delta IP_i(R)$ accounts for the shift in the ionization potential due to the interactions between the molecular target and the probe.

$$\Delta IP_i = V^*(\infty) - V_i^+(\infty) - [V^*(R) - V_i^+(R)] \qquad (3)$$

The anisotropy of the interaction potential curve V^* describing the approach of the He*(2^3S) probe toward the molecular target along various directions has been calculated on the basis of the well-known resemblance[22−24] between the He*(2^3S) and Li(2^2S) species in collision processes.

In this way, to obtain information on anisotropic interaction between He*(2^3S) and various molecules with chemical functional groups, many materials were investigated in our group in recent years.[25] The obtained results allow us to determine some tendencies in the anisotropic interaction with He*(2^3S); attractive interaction around lone-pair electrons,[26−28] π-regions of unsaturated hydrocarbons[26] and heterocyclic compunds,[29] or repulsive interaction around C−H bonds of alkyl groups.[30]

In this study, 2D-PIES of formic acid (HCOOH), acetic acid (CH_3COOH), and its structural isomer, methyl formate ($HCOOCH_3$), were observed. Attractive interactions around the oxygen atoms and steric hindrance caused by repulsive interactions around the methyl groups are interesting in CEDPICS and Penning ionization reactivity for similar compounds.

II. Experimental Section

The experimental apparatus used for the measurement has been described in detail many times in previous papers.[14−17,25] Briefly, the metastable He*(2^3S) atoms were produced by the discharge nozzle source at a pressure of about 60 Torr. As a byproduct of this discharge, the metastable He*(2^1S) were generated, and they were quenched by the water-cooled helium discharge lamp. To obtain the collision energy dependent spectra, the metastable helium atom beam was modulated on the way to the target molecule by a random chopper[31] disk rotated with a frequency of about 400 Hz. For the UPS measurement, the UPS photons from the HeI resonance line (584 Å, 21.22 eV) are also generated by the discharge in pure helium gas.

The kinetic energy of ejected electrons was measured by a hemispherical electrostatic deflection type analyzer[25] at the detection angle of 90°. The energy resolution was determined by the measurement of the full width at half-maximum (fwhm) of the Ar^+ ($^2P_{3/2}$) peak. The UPS and PIES spectra from high-resolution mode have the value of fwhm of about 40 meV, and the 2D-PIES data were obtained at a resolution less than 250 meV. The transmission curve of the energy analyzer was determined by comparing of our peak intensity data with those from well-known UPS data.[32,33]

The collision energy dependence of the ionization cross sections can be obtained for a specific ionic state in 2D-PIES. In the 2D-PIES measurement, the TOF spectrum I_E at a scanning kinetic energy was accumulated. For the determination of the He*(2^3S) velocity ν_M, another measurement of the TOF spectrum of He*(2^3S) I_M by detecting secondary electrons from a stainless metal plate inserted into the collision cell was employed. The partial ionization cross section $\sigma(E_e,\nu_R)$ can be determined by the equations:

$$\sigma(E_e,\nu_R) = c(I_E(E_e,\nu_M)/I_M(\nu_M))(\nu_M/\nu_R) \qquad (4)$$

$$\nu_R = (\nu_M{}^2 + 3k_BT/m)^{1/2} \qquad (5)$$

where c is a constant, ν_R is the relative velocity of collision adjusted for the average velocity of the target molecules with mass m at temperature T, and k_B is the Boltzmann constant. Finally, $\sigma(\nu_R)$ is converted to $\sigma(E_c)$ by the relationship

$$E_c = \mu\nu_R{}^2/2 \qquad (6)$$

where μ is the reduced mass of the system.

III. Calculations

The difficulties of the calculation for excited states can be avoided by using the resemblance between the metastable He*(2^3S) and Li(2^2S) atom as mentioned in the Introduction. The interaction potential $V(R)$ between a molecule and the approaching Li(2^2S) can be obtained by ab initio MO calculations, where R is the distance from the Li atom to the investigated part of the molecule. The calculations of $V(R)$ were carried out with use of the second-order Møller−Plesset perturbation theory (MP2) with the standard 6-311+G** basis set. Moreover, to correct the basis-set superposition errors (BSSE), the full counterpoise (CP)[34] method was used.

The ionization potentials of an isolated target molecule were calculated with high accuracy by the outer valence Green's function (OVGF) method.[35,36] In addition, a restricted Hartree−Fock (RHF) method was performed to obtain the electron density maps.

All presented ab initio calculations were performed with the Gaussian 03 quantum chemistry package.[37] The molecular geometry for these calculations was selected from experimental data[38−40] based on the microwave spectroscopy in cases for formic and acetic acids and on the gas-phase electron diffraction results for methyl formate.

IV. Results

Figures 1−3 show the ultraviolet photoelectron spectrum (UPS), Penning ionization electron spectrum (PIES), as well as collision-energy-resolved PIES of formic acid (HCOOH), acetic acid (CH_3COOH), and methyl formate ($HCOOCH_3$). The scales of the electron kinetic energy for PIES are shifted relative to those for UPS by the difference of the excitation energies, 21.22 eV − 19.82 eV = 1.40 eV. In CERPIES, solid lines show lower-collision-energy spectra in the range from 70 to 110 meV (average 90 meV) and dashed lines show higher-collision-energy spectra in the range from 200 and 270 meV (average 235 meV). The relative intensities of low-energy to high-energy spectra are normalized by using the data of $\log(\sigma)$ versus $\log(E_c)$ plots.

Figures 1−3 present the general form of the spectra of investigated molecules. All the peaks are numbered in ascending order starting with the peak at the lowest ionization potential. The assignments of peaks were made mainly on the basis of OVGF calculation. When one follows the peak position from UPS to PIES, it is possible to notice that the ionization potential is changing for some peaks. This effect is concerned with a known fact, that the kinetic energy of an emitted electron in PIES is equal to the difference between two curves for the entrance (the curve of interaction potential $V^*(R)$) and the exit channels as mentioned in the Introduction. If the potential energy curve for the exit channel can be assumed to be flat, the energy for the exit channel can be determined from IPs by UPS. The peak energy shift, therefore, reflects the anisotropic character of interaction between a He*(2^3S) atom and the target molecule at the spatial region where MO is extending and electron

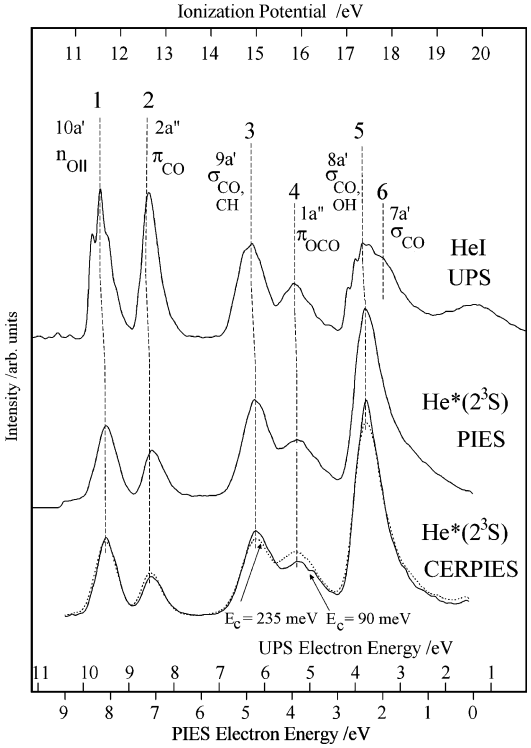

Figure 1. HeI UPS, He*(2^3S) PIES, and collision-energy-resolved He*(2^3S) Penning ionization electron spectra (CERPIES) of HCOOH (dashed curve at 235 meV, solid curve at 90 meV).

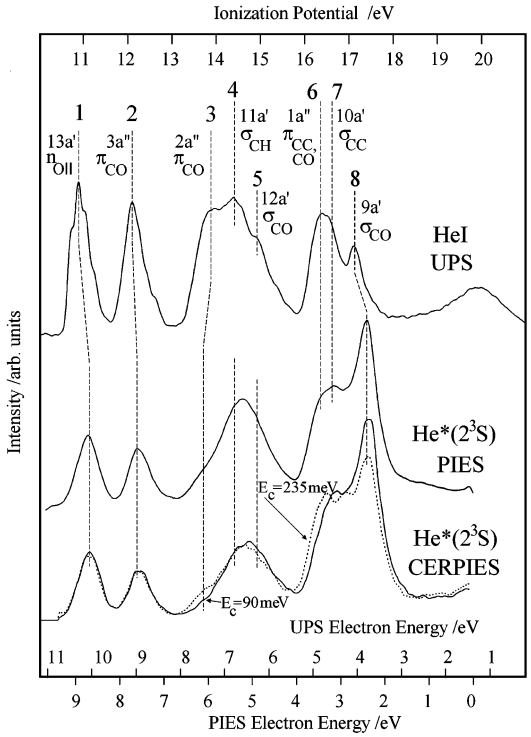

Figure 2. HeI UPS, He*(2^3S) PIES, and CERPIES of CH_3COOH (dashed curve at 235 meV, solid curve at 90 meV).

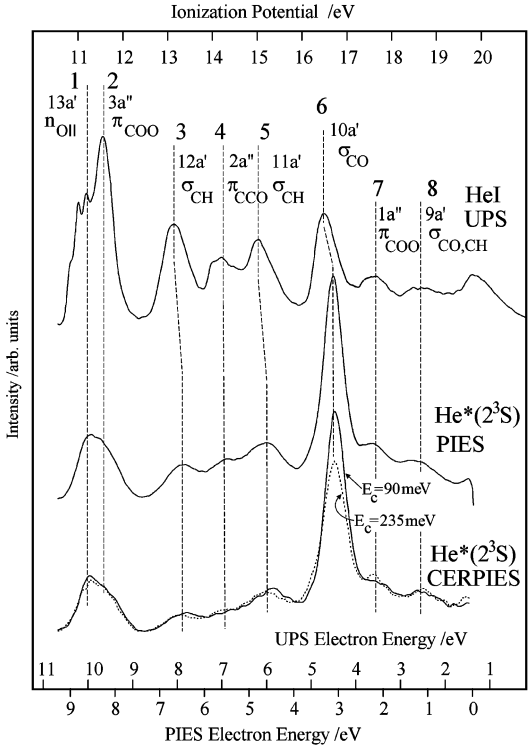

Figure 3. HeI UPS, He*(2^3S) PIES, and CERPIES of $HCOOCH_3$ (dashed curve at 235 meV, solid curve at 90 meV).

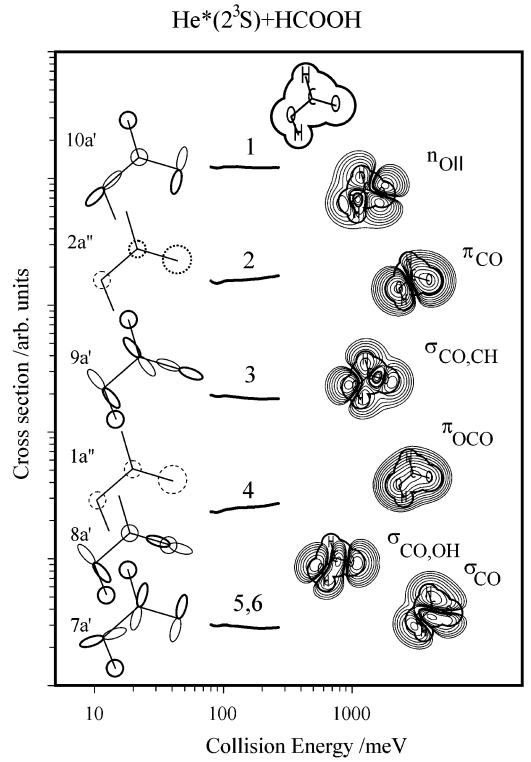

Figure 4. Collision energy dependence of the partial ionization cross section for HCOOH with He*(2^3S).

transition occurs. Since all potential energy surfaces for the exit channels cannot be assumed to be flat, quantitative discussions on the potential energy surface of the entrance channel are thought to be difficult by the negative or positive peak energy shift.

The anisotropy of interaction potential can be reflected in CERPIES; the negative change of peak height between spectra from low collision energy (solid lines) to high collision energy (dashed lines) indicates the attractive interaction. Thus it may be useful to show the CERPIES next to PIES/UPS in Figures 1−3. As long as the three kinds of spectra were obtained by different experiments, the reliability of the results increased.

Figures 4−6 show the CEDPICS by $\log(\sigma)$ vs $\log(E_c)$ plots and the calculated electron density maps together with the schematic representation of MOs for HCOOH, CH_3COOH, and $HCOOCH_3$, respectively. The O−C═O plane (molecular plane)

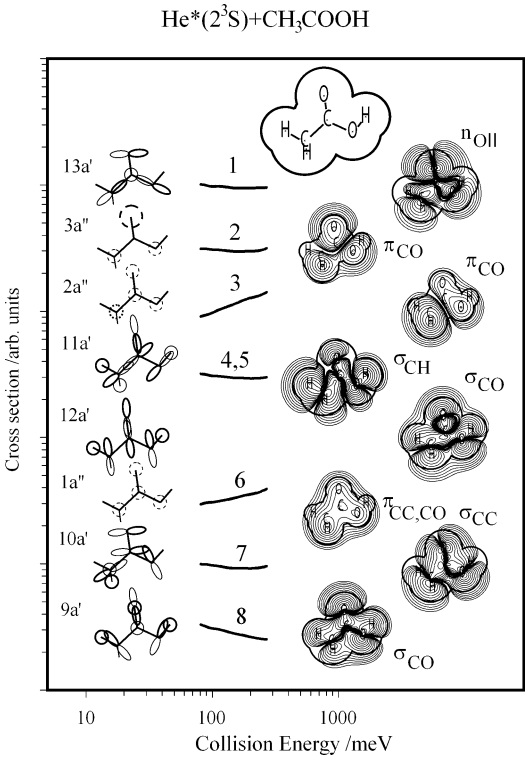

Figure 5. Collision energy dependence of the partial ionization cross section for CH_3COOH with He*(2^3S).

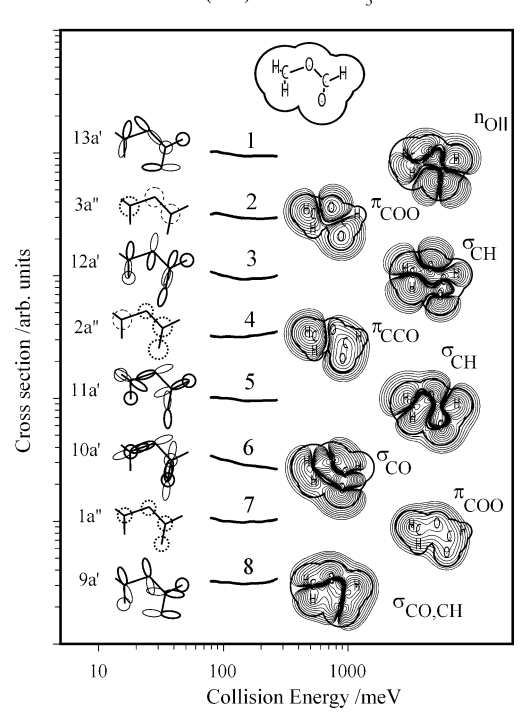

Figure 6. Collision energy dependence of the partial ionization cross section for $HCOOCH_3$ with He*(2^3S).

was selected as the cutting plane for the electron density maps. For π orbtials, the cutting plane is 1.0 Å above the molecular plane.

The experimental data were listed in the Table 1 for three investigated molecules. The first three columns show the name of the molecules, the band number (ordered as in the previous figures), and the molecular orbital character. The next two columns show the ionization potentials (IPs) by OVGF calculation and UPS. The positions of some peaks were determined by the approximation of spectra with Gauss curves, and IP values in this case are marked with an asterisk (∗). The column of peak energy shift (ΔE) shows the difference of peak position in PIES relative to the corresponding UPS peaks taking the excitation energy difference for PIES and UPS into consideration ($21.22-19.82 = 1.4$ eV). Slope values of the CEDPICS obtained by the least-squares method in the collision energy range of 90−270 meV are also listed in Table 1.

TABLE 1: Band Assignment, Ionization Potential (IP), Peak Energy Shift (ΔE), and Slope Parameter (m) of CEDPICS

molecule	band	orbital character	IP OVGF/ eV	IP UPS/ eV	ΔE/ eV	m
HCOOH	1	$n_{OII}(10a')$	11.69	11.51	−0.09	0.01
(formic acid)	2	$\pi_{CO}(2a'')$	12.67	12.60	−0.06	0.09
	3	$\sigma_{CO,CH}(9a')$	15.17	14.90	−0.06	−0.06
	4	$\pi_{OCO}(1a'')$	16.06	15.82	−0.08	0.16
	5	$\sigma_{CO,OH}(8a')$	17.94	17.36	−0.04	−0.06
	6	$\sigma_{CO}(7a')$	18.12	17.82*		
CH_3COOH	1	$n_{OII}(13a')$	11.06	10.87	−0.21	−0.05
(acetic acid)	2	$\pi_{CO}(3a'')$	12.19	12.09	−0.11	−0.03
	3	$\pi_{CO}(2a'')$	14.19	13.79*	0.07	0.37
	4	$\sigma_{CH}(11a')$	14.59	14.39		−0.06
	5	$\sigma_{CO}(12a')$	14.75	14.94		
	6	$\pi_{CC,CO}(1a'')$	16.44	16.38		0.21
	7	$\sigma_{CC}(10a')$	16.84			−0.06
	8	$\sigma_{CO}(9a')$	17.58	17.08	−0.28	−0.22
$HCOOCH_3$	1	$n_{OII}(13a')$	11.36	11.09*	−0.09	−0.08
(methyl formate)	2	$\pi_{COO}(3a'')$	11.68	11.59	−0.03	−0.09
	3	$\sigma_{CH}(12a')$	13.44	13.14	−0.19	−0.10
	4	$\pi_{CCO}(2a'')$	14.53	14.17	−0.02	0.06
	5	$\sigma_{CH}(11a')$	15.09	15.04	−0.14	−0.05
	6	$\sigma_{CO}(10a')$	17.07	16.49	−0.21	−0.20
	7	$\pi_{COO}(1a'')$	16.77	17.64	0.06	0.05
	8	$\sigma_{CO,CH}(9a')$	18.36	18.68	0.06	0.00

The calculated interaction potential curves by MP2/6-311+G** around the carbonyl and hydroxyl oxygen atoms are presented in Figures 7 (out-of-plane direction) and 8 (in-plane direction) as a function of angle. The distance between Li(2^2S) and the oxygen atom was fixed at 2.1 Å, which roughly corresponds to the interatomic distance for the bottom of the interaction potential well. For the out-of-plane directions, the angle was determined on the additional intersecting planes along the carbonyl axis or bisect lines of the COH (or COC) angle as shown in Figure 7. For in-plane directions, the angle was determined from the carbon atom of carbonyl bonds or the H (or C) atom of hydroxyl (or methoxyl) bonds on the molecular plane as shown in Figure 8.

V. Discussion

In the case of attractive interaction with atomic targets, its long-range attractive (R^{-s}) part can be approximated by relation:

$$V^*(R) \sim R^{-s} \tag{7}$$

The collision energy dependence of ionization cross sections can be represented[2,4,9] by

$$\sigma(E_c) \sim E_c^{-2/s} \tag{8}$$

or in the following form:

$$\log(\sigma(E_c)) \sim -2/s \log(E_c) \tag{9}$$

The slope parameter m of CEDPICS for the $\log(\sigma)$ vs $\log(E_c)$ plots are shown in the Table 1.

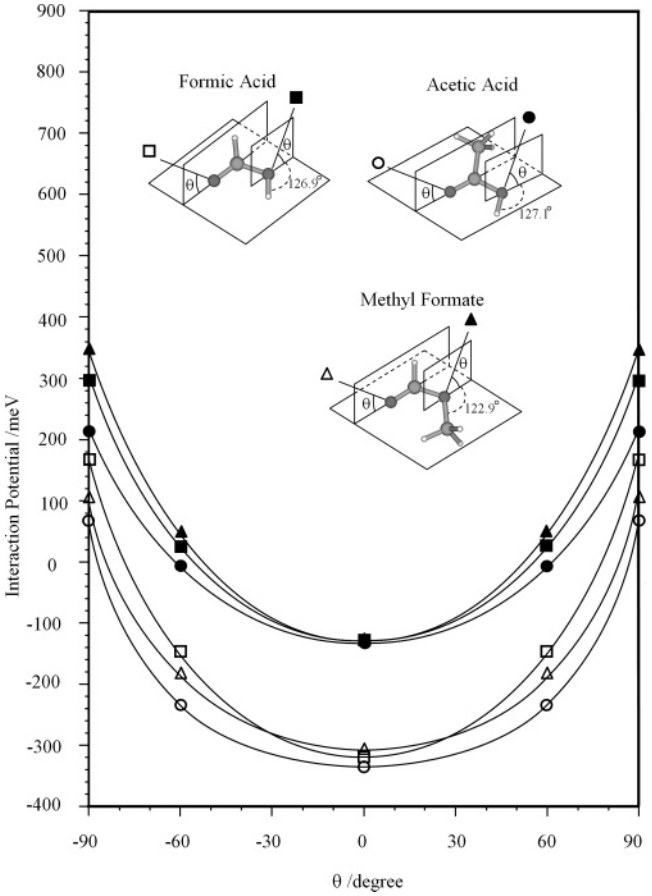

Figure 7. Interaction potential energy curves of out-of-plane directions on the molecular plane as a function of angle θ from the molecular plane. □, ○, △ and ■, ●, ▲ indicate the interaction potential around the carbonyl and hydroxyl oxygen atoms for HCOOH, CH_3COOH, and $HCOOCH_3$, respectively. The distance between Li(2^2S) and the oxygen atom was fixed at 2.1 Å.

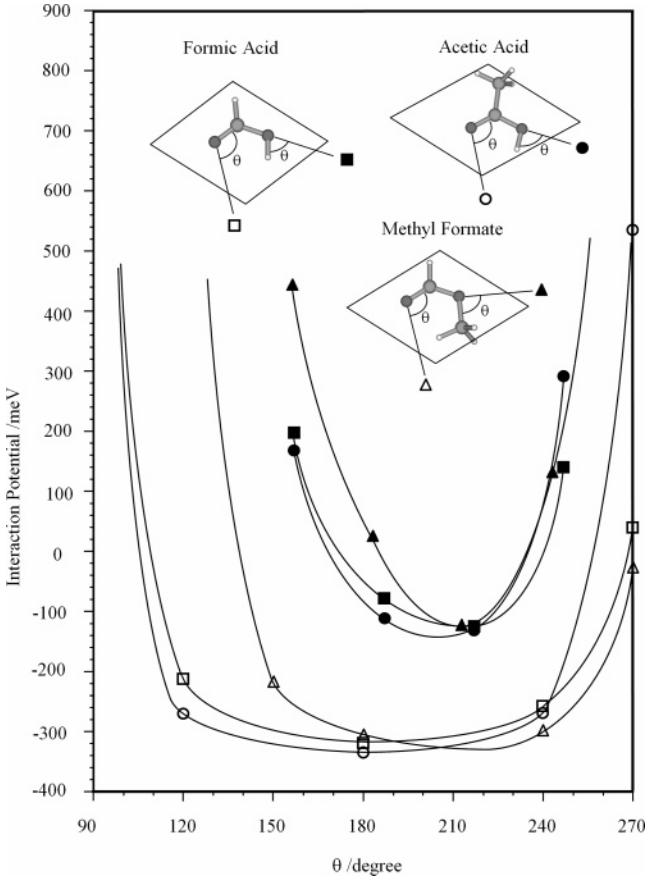

Figure 8. Interaction potential energy curves of in-plane directions on the molecular plane as a function of angle θ from the carbonyl C═O axis or the hydroxyl OH (methoxyl OC) axis. □, ○, △ and ■, ●, ▲ indicate the interaction potential around the carbonyl and hydroxyl oxygen atoms for HCOOH, CH_3COOH, and $HCOOCH_3$, respectively. The distance between Li(2^2S) and the oxygen atom was fixed at 2.1 Å.

HCOOH. The OVGF calculation resulted in six ionic states for valence ionization of HCOOH. Figure 1 shows five distinct bands in PIES. In UPS, band 6 ($\sigma_{CO}(7a')$) can be noticed close to band 5, but in PIES this band 6 is concealed by a strong band 5 ($\sigma_{CO,OH}(8a')$). A relatively large intensity for the σ_{CO} orbital localized mostly around the C═O bond was observed for several compounds in PIES,[26,41] which can be explained by the large extension of electron density outside the molecular surface for σ_{CO} MOs.

The comparison of bands 1 and 2 in UPS and PIES shows a relative decreasing of intensity for band 2 in PIES. Since Penning ionzation probability is governed by overlap between the helium 1s orbital and target MOs and vanished at nodal planes, the intensity difference in PIES can be explained by the electron density distribution and nodal planes of corresponding MOs. In the case of band 1 and band 2, the $\pi_{CO}(2a'')$ MO (band 2) has two nodal planes for in-plane and out-of-plane directions, while the $n_{O||}(10a')$ MO (band 1) is in-phase outside the molecular surface and has one nodal plane for the out-of-plane direction, which is the main reason of the intensity difference in PIES.

As indicated in Figure 4, band 1 ($n_{O||}(10a')$) has a small slope close to zero in CEDPICS. In previous studies, interactions with He* around an oxygen atom appear attractive in the lone pair electron region, and corresponding CEDPICS showed negative slope values.[26−28] In the case of HCOOH in this study, the electron density of $n_{O||}$ extends around the H atoms, which can have a relationship with the CEDPICS of band 1 by repulsive interaction around H atoms. A similar case was investigated for formamide ($HCONH_2$).[42]

Bands 3 ($\sigma_{CO,CH}(9a')$) and 5 ($\sigma_{CO,OH}(8a')$) showed negative slopes of CEDPICS ($m = -0.06$), while ionization from the $n_{O||}$ MO showed a zero slope of CEDPICS as mentioned above. This difference can be ascribed to strong attraction for the σ_{CO} orbital region as shown in the results of model potential calculations for the C═O axis direction (Figures 7 and 8).

The m values of CEDPICS for bands 2 and 4 are positive: 0.09 and 0.16. Both of these bands correspond to π-type MO: $\pi_{CO}(2a'')$ and $\pi_{OCO}(1a'')$. The repulsive character of interaction around the π-orbital region was observed for amides.[42]

Figures 7 and 8 show the interaction potential between a formic acid molecule and a Li atom. The calculated interaction has an attractive nature in the regions around the oxygen atoms. This result indicates that the most important area for the attractive interaction is near the carbonyl oxygen atom and that the well depth around the oxygen atom reaches the value of −319 meV. The attractive area localizes along the C═O axis with a cone shape whose vertex is near the carbonyl oxygen. The opening angle of this cone can reach ca. 140−150°. For another oxygen atom in the hydroxyl group, the smaller well depth (−127 meV) and smaller opening angle of the attractive interaction zone (∼60° in plane of molecule) may result in a smaller degree of attractive interactions between HCOOH and He*.

Taking the large band intensity in PIES for ionization from σ_{CO} MOs into consideration, the electron density extension of

σ_{CO} MOs is relatively large and, thus, the large interorbital interaction between the σ_{CO}-type MO and valence orbital of He*(2s) can result in attractive interaction around the σ_{CO} bond and a negative slope of CEDPICS. In the opposite way, electron density extension of π MOs may be smaller than σ_{CO} MOs, which can be connected with repulsive interaction around the π MO region.

CH_3COOH. UPS and PIES of acetic acid are shown in Figure 2. Overlapping bands 4 ($\sigma_{CH}(11a')$) and 5 ($\sigma_{CO}(12a')$) cannot be separated in PIES, and the IP values by OVGF calculation also exhibit a small difference (~0.16 eV) in reversed order from MO energy (Koopmans' IP) order. Bands 6 ($\pi_{CC,CO}(1a'')$) and 7 ($\sigma_{CC}(10a')$) are also close each other. Ionization from σ_{CO} MO shows strong intensity for band 5 in PIES relative to UPS similar to that for band 5 ($\sigma_{CO,OH}(12a')$) of HCOOH.

The large intensity of band 8 in PIES can be assigned to ionization from the $\sigma_{CO}(9a')$ MO, which is consistent with OVGF calculation, a large negative slope of CEDPICS ($m = -0.22$), as well as a negative peak energy shift ($\Delta E = -0.28$ eV). The model potential calculations show similar attractive interaction around the oxygen atoms for CH_3COOH (Figures 7 and 8) and HCOOH. The well depth around the carbonyl group and the hydroxyl group is −336 and −131 meV, respectively.

The largely overlapping bands 4 and 5 are both related to $\sigma_{CO}(12a')$ and $\sigma_{CH}(11a')$ MO distributions for in-plane directions. In CERPIES, a negative collision energy dependence of band intensity was observed for band 5, which should be assigned to the strong attractive interaction around the carbonyl group in ionization from the $\sigma_{CO}(12a')$ MO. The small negative slope of CEDPICS for the sum of bands 4 and 5 can be ascribed to the attractive interaction around the σ_{CO} region as well as repulsive interaction around the $\sigma_{CH}(11a')$ MO region. Thus, ionic states for bands 4 and 5 are reasonably assigned to 11a′ MO and 12a′ MO, respectively.

Despite the similar $n_{O||}$ MO character, band 1 of CH_3COOH showed negative CEDPICS ($m = -0.05$), which is smaller than that of band 1 for HCOOH (10a′ MO, $m = 0.01$). This difference can be ascribed to the electron density of the 13a′ MO of CH_3-COOH around the methyl group. In the case of HCOOH, the H atom has a 1s atomic orbital component and is favorable in ionization, while the C atom of the methyl group has a 2p component and is out-of-phase around the methyl group. The small negative slope of band 7 ($\sigma_{CC}(10a')$) can be explained similarly.

The smaller intensity of bands 2 ($\pi_{CO}(3a'')$) and 3 ($\pi_{CO}(2a'')$) than band 1 ($n_{O||}(13a')$) in PIES can be ascribed to the electron density distribution and nodal planes as is the case with HCOOH. Band 3 ($\pi_{CO}(2a'')$) in PIES has a positive intensity increasing in CERPIES as well as CEDPICS (Figure 5) and a positive peak energy shift ($\Delta E \sim +0.07$ eV), which indicates repulsive interaction for the $\pi_{CO}(2a'')$ MO region corresponding to band 3. A large positive slope of CEDPICS was observed for band 6 corresponding to ionization fromthe $\pi_{CC,CO}(1a'')$ MO. The absolute values of positive slope of CEDPICS for band 3 ($m = +0.37$) and band 6 ($m = +0.21$) are larger than those for π bands of HCOOH, which can be explained by the electron distribution of π MOs around the methyl group in CH_3COOH and repulsive interaction around the methyl group. As for band 2 corresponding to the $\pi_{CO}(3a'')$ MO, it can be supposed that the $\pi_{CO}(3a'')$ MO is distributing in both attractive and repulsive regions and both interaction types are compensating, which can result in a neutral effective potential of collision and the small slope value of CEDPICS ($m = -0.03$). By the model potential calculations, the attractive area localizes mostly in-plane directions around the oxygen atoms.

It is interesting that one can find a similarity in behavior of CEDPICS for some bands of formic acid (HCOOH) and acetic acid (CH_3COOH) with those of formamide ($HCONH_2$) and acetamide (CH_3CONH_2);[42] repulsive interactions were found for π_{NCO} MOs of amides, while the slope of CEDPICS for the $n_{O||}$ orbital is near zero for formamide and weakly negative for acetamide. This similarity may be due to the structural relationship between acids and amides. From the slope values of CEDPICS, interaction between metastable atoms and formamide or acetamide showed more attractive character rather than formic acid or acetic acid. A similar change in interaction for out-of-plane directions was investigated for furan (C_4H_4O) and pyrrole (C_4H_5N).[29]

$HCOOCH_3$. In Figure 3, UPS and PIES of methyl formate were shown. For the relative band intensity of band 1 and band 2, band 2 has a larger intensity than band 1 in UPS, while band 1 is larger than band 2 in PIES, which can be explained by the electron density distribution and nodal planes of the $n_{O||}(13a')$ MO for band 1.

As for the assignment of observed bands 6 and 7, band 6 in PIES can be assigned to ionization from a σ_{CO}-type MO based on the large intensity, large negative collision energy dependence in CEDPICS (Figure 6) and CERPIES, as well as the large negative peak energy shift ($\Delta E = -0.21$ eV), which is different from the small intensity and positive CEDPICS of band 7. By the attractive interaction obtained from model potential calculations (Figures 7 and 8) and the similarity with HCOOH and CH_3COOH, band 6 is confirmed to occur from ionization from $\sigma_{CO}(10a')$ despite the inconsistency with IP order by OVGF calculation ($\pi_{COO}(1a'') < \sigma_{CO}(10a')$) with the energy difference of 0.30 eV.

Ionization bands corresponding to π MOs show relatively small intensity and positive (bands 4 and 7) or small negative (band 2) slope values in CEDPICS. The negative slope value of band 2 can be ascribed to the electron density distribution of the $\pi_{COO}(3a'')$ MO mainly for out-of-plane directions around the C═O group, which is similar to the case for the 3a″ MO of CH_3COOH.

Ionization from σ MOs shows the following three interesting features:

(1) CEDPICS for band 3 ($\sigma_{CH}(12a')$) shows a bending shape with a negative slope in the 80−150 meV region and a positive slope in the 150−270 meV region, which can be due to the sum of attractive interaction around the oxygen atoms of the carbonyl group as well as the methoxyl group and repulsive interaction around the CH_3 group for ionization from the 12a′ MO,

(2) CERPIES for band 6 ($\sigma_{CO}(10a')$) shows larger intensity for the higher collision energy (dashed curve) in the higher electron energy region of band 6 around 3.6 eV in electron energy (Figure 3) and the slope value of this electron energy region is positive ($m = +0.14$), which can be ascribed to the ionization from the 10a′ MO around the methyl group because electron energy is larger for ionization in the repulsive interaction region from the two-curve model mentioned in the Introduction.

(3) CEDPICS for band 8 shows a slope value of zero despite the in-plane extension of the corresponding $\sigma_{CO,CH}(9a')$ MO, which can be understood by the nodal plane along the C═O axis where ionization probability with strongly attracted He* atoms vanishes.

The model potential calculations for $HCOOCH_3$−Li indicate similarity and difference with those for formic acid and acetic acid. The similar point is that attractive interaction around the carbonyl oxygen (−304 meV) is much larger than that around the oxygen atom (−124 meV) of the methoxyl group. On the other hand, the different point is that the attractive interaction area around the two oxygen atoms is not so wide as that of acid compounds due to the steric hindrance by the methyl group. Actually, the attractive area is limited and the repulsive interaction was calculated for the access of Li to the oxygen atom of the carbonyl group along the 120° line from the C═O axis near the methyl group on the molecular plane, while attractive interaction was calculated for the same direction for formic acid and acetic acid. For attractive interaction around the oxygen atom of the methoxyl group, steric hindrance by hydrogen atoms of methyl and the formyl group makes the attractive area narrower compared with the cases of formic acid and acetic acid. These effects of steric hindrance by the methyl group can result in smaller absolute values of CEDPICS for ionization of $HCOOCH_3$ rather than HCOOH and CH_3COOH.

VI. Conclusion

Anisotropic interactions around HCOOH, CH_3COOH, and $HCOOCH_3$ have been investigated by collision-energy/electron-energy-resolved two-dimensional Penning ionization electron spectroscopy as well as model calculations of interaction potential between the target molecule and He(2^3S) metastable atoms.

Strong attractive interactions were found for ionization from σ_{CO} MOs by observation of collision energy dependence of partial ionization cross sections, while repulsive interactions were obtained for out-of-plane directions and around hydrogen atoms of methyl groups or formyl groups. These anisotropic interactions are consistent with the results from model calculations of the interactions, using a Li(2^2S) atom in place of He*(2^3S), and the well depth of the interaction potential around the carbonyl group was more than 300 meV. Band 6 in PIES of $HCOOCH_3$ was assigned to ionization from σ_{CO} orbital experimentally because of the large negative peak energy shift and negative collision energy dependence as well as large band intensity.

Different from σ_{CO} bands, π bands have less relative intensity in PIES compared to UPS that can be explained by nodal planes of electron density distribution of corresponding π MOs and repulsive interaction around the π orbital region, which is similar to amide compounds, formamide ($HCONH_2$), as well as acetamide (CH_3CONH_2).[42]

The structural difference between CH_3COOH and its isomer $HCOOCH_3$ was reflected in the steric hindrance by the methyl group around the carbonyl group and the formyl group of $HCOOCH_3$, which was found for slopes of CEDPICS and interaction potential calculation results compared with those for CH_3COOH.

Acknowledgment. The present work was supported by a Grant-in-Aid for Scientific Research from the Japanese Ministry of Education, Culture, Sports, Science and Technology. A.B. is supported by the Research Fellowship of the Japan Society for the Promotion of Science for a JSPS postdoctoral fellowship (ID: P04384). M.Y. is supported by the Research Fellowship of the Japan Society for the Promotion of Science for Young Scientists.

References and Notes

(1) Penning, F. M. *Naturwissenschaften* **1927**, *15*, 818.
(2) Niehaus, A. *Adv. Chem. Phys.* **1981**, *45*, 399.
(3) Yencha, A. J. *Electron Spectroscopy*: *Theory, Techniques and Applications*; Brundle, C. R., Baker, A. D., Eds.; Academic: New York, 1984; Vol. 5.
(4) Illenberger, E.; Niehaus, A. *Z. Phys. B* **1975**, *20*, 33.
(5) Parr T. P.; Parr, D. M.; Martin, R. M. *J. Chem. Phys.* **1982**, *76*, 316.
(6) Pesnelle, A.; Watel, G.; Manus, C. *J. Chem. Phys*. **1975**, *62*, 3590.
(7) Woodard, M. R.; Sharp, R. C.; Seely, M.; Muschlitz, E. E., Jr. *J. Chem. Phys*. **1978**, *69*, 2978.
(8) Appolloni, L.; Brunetti, B.; Hermanussen, J.; Vecchiocattivi, F.; Volpi, G. G. *J. Chem. Phys*. **1987**, *87*, 3804.
(9) Allison, W.; Muschlitz, E. E., Jr. *J. Electron Spectrosc. Relat. Phenom*. **1981**, *23*, 339.
(10) Riola, J. P.; Haward, J. S.; Rundel, R. D.; Stebbings, R. F. *J. Phys. B* **1974**, *7*, 376.
(11) Lindinger, W.; Schmeltekopf, A. L.; Fehsenfeld, F. C. *J. Chem. Phys.* **1974**, *61*, 2890.
(12) Hotop, H.; Niehaus, A. *Z. Phys.* **1969**, *228*, 68.
(13) Čermák, V. *J. Chem. Phys.* **1966**, *44*, 3781.
(14) Mitsuke, K.; Takami, T.; Ohno, K. *J. Chem. Phys*. **1989**, *91*, 1618.
(15) Ohno, K.; Takami, T.; Mitsike, K.; Ishida, T. *J. Chem. Phys*. **1991**, *94*, 2675.
(16) Takami, T.; Mitsike, K.; Ohno, K. *J. Chem. Phys*. **1991**, *95*, 918.
(17) Takami, T.; Ohno, K. *J. Chem. Phys*. **1992**, *96*, 6523.
(18) Dunlavy, D. C.; Martin, D. W.; Siska, P. E. *J. Chem. Phys*. **1990**, *93*, 5347.
(19) Longley, E. J.; Dunlavy, D. C.; Falcetta, M. F.; Bevsek, H. M.; Siska, P. E. *J. Phys. Chem.* **1993**, *97*, 2097.
(20) Siska, P. E. *Rev. Mod. Phys.* **1993**, *65*, 337.
(21) Ohno, K.; Yamakado, H.; Ogawa, T.; Yamata, T. *J. Chem. Phys*. **1996**, *105*, 7536.
(22) Rothe, E. W.; Neynaber, R. H.; Trujillo, S. M. *J. Chem. Phys*. **1965**, *42*, 3310.
(23) Hotop, H. *Radiat. Res.* **1974**, *59*, 379.
(24) Haberland, H.; Lee, Y. T.; Siska, P. E. *Adv. Chem. Phys*. **1981**, *45*, 487.
(25) E.g.: Ohno, K. *Bull. Chem. Soc. Jpn.* **2004**, *77*, 887.
(26) Ohno, K.; Okamura, K.; Yamakado, H.; Hoshino, S.; Takami, T.; Yamauchi, M. *J. Phys. Chem.* **1995**, *99*, 14247.
(27) Pasinszki, T.; Kishimoto, N.; Ohno, K. *J. Phys. Chem. A* **1999**, *103*, 9195.
(28) Kishimoto, N.; Osada, Y.; Ohno, K. *J. Phys. Chem. A* **2000**, *104*, 1393.
(29) Kishimoto, N.; Yamakado, H.; Ohno, K. *J. Phys. Chem.* **1996**, *100*, 8204.
(30) Yamakado, H.; Yamauchi, M.; Hoshino, S.; Ohno, K. *J. Phys. Chem.* **1995**, *99*, 17093.
(31) Kishimoto, N.; Aizawa, J.; Yamakado, H.; Ohno, K. *J. Phys. Chem. A* **1997**, *101*, 5038.
(32) Gardner, J. L.; Samson, J. A. R. *J. Electron Spectrosc. Relat. Phenom*. **1976**, *8*, 469.
(33) Kimura, K.; Katsumata, S.; Achiba, Y.; Yamazaki, T.; Iwata, S. *Handbook of HeI Photoelectron Spectra of Fundamental Organic Molecules*; Japan Scientific: Tokyo, Japan, 1981.
(34) Boys, S. F.; Bernardi, F. *Mol. Phys.* **1970**, *19*, 553.
(35) Cederbaum, L. S.; Domcke, W. *Adv. Chem. Phys.* **1977**, *36*, 205.
(36) Ortiz, J. V. *J. Chem. Phys.* **1996**, *104*, 7599.
(37) Frisch, A. et al. *Gaussian 03*, Revision C.02; Gaussian, Inc.: Wallingford, CT, 2004.
(38) Tam, H. S.; Choe, J. I.; Harmony, M. D. *J. Phys. Chem.* **1991**, *95*, 9267.
(39) van Eijck, B. P.; van Opheusden, J.; van Schaik, M. M. M.; van Zoeren, *E. J. Mol. Spectrosc.* **1981**, *86*, 465.
(40) Cradock, S.; Rankin, D. W. H. *J. Mol. Struct.* **1980**, *69*, 145.
(41) Ohno, K.; Takano, S.; Mase, K. *J. Phys. Chem.* **1986**, *90*, 2015.
(42) Kishimoto, N.; Osada, Y.; Ohno, K. *J. Electron Spectrosc. Relat. Phenom*. **2001**, *114*−*116*, 183.